June 12-16, 2023, New Brunswick, New Jersey

MSEC2023-104610

RAPID 3D PRINTING OF NANOPOROUS COPPER POWDERS VIA MICRO-CLIP

Luyang Liu School of Manufacturing Systems and Networks, Arizona State University, Mesa, AZ

Natalya Kublic School of Manufacturing Systems and Networks, Arizona State University, Mesa, AZ *Correspondence: Xiangfan.Chen@asu.edu

Bruno Azeredo School of Manufacturing Systems and Networks, Arizona State University, Mesa, AZ

Xiangfan Chen* School of Manufacturing Systems and Networks, Arizona State University, Mesa, AZ

ABSTRACT

Three-dimensional (3D) printing of metal components has attracted broad interest continuously. The printing methods include selective laser sintering, fused deposition modeling, vat photopolymerization, etc. Particularly, 3D printing of metal components via material extrusion or vat photopolymerization usually utilizes metal particle-reinforced polymer matrix composites (PMCs) as raw materials. However, the resolution for material extrusion-based printing is limited, and the printing speed is relatively slow due to the voxel-by-voxel scanning nature. Though the vat photopolymerization can significantly increase the printing resolution and speed simultaneously, the filler loading of the PMC suitable for vat photopolymerization is typically low due to the critical requirement on rheological properties of printable resins. Herein, we develop a new metal 3D printing strategy by introducing nanoporous copper (NP-Cu) powders with significantly increased surface area into the photocurable polymer matrix. The composition of the PMC resins was optimized by balancing the need for higher filler loading, and the requirements on resins' rheological properties from the resin's stabilization and replenishment during the customized micro-continuous liquid interface printing ($\mu CLIP$). The concentration of the NP-Cu powders in the PMC resins can reach up to 40 wt% without sacrificing the printability and printing speed of µCLIP. We have successfully printed 3D structures with resolution of 5.8 µm·pixel⁻¹ and printing speed of 10 μm·s⁻¹. Moreover, 3D copper structures can be realized after sintering, and the structures manifest an average resistivity of 150 kΩ·mm at room temperature. In summary, we explored a new

strategy, which can potentially benefit the rapid printing of sophisticated 3D metal structures with higher resolution and shorter fabrication time.

Keywords: micro-continuous liquid interface printing, nanoporous copper powders, high resolution.

1. INTRODUCTION

(3D) metal Three-dimensional components with customized geometries have been broadly applied in the construction, aerospace, and automotive industries [1]. To fabricate customized 3D metal structures featuring sophisticated geometries, various additive manufacturing (also known as 3D printing) technologies, including selective laser sintering (SLS), direct energy deposition (DED), metal binder jetting (BJ), fused deposition modeling (FDM), and vat photopolymerization (VP), have rapidly evolved and been utilized in the last two to three decades [2]. Particularly, 3D printing technologies such as material extrusion and vat photopolymerization, which utilize metal particle-reinforced polymer matrix composites (PMCs) as raw materials, provide new opportunities [3]. Compared to other technologies like SLS [4], DED [5], and BJ [6], the aforementioned methods offer many advantages, such as lower cost, tabletop systems, and reduced operation hazards [2]. However, for material extrusion-based processes, e.g., FDM, the printing resolution is limited by the nozzle size ($\sim 100 \, \mu m$ to $\sim 1.2 \, m$ mm), and the printing speed is relatively slow because of the voxel-by-voxel scanning nature. On the other hand, the VPbased 3D printing processes, such as stereolithography (SLA) [7,8] utilizing focused UV laser beam, projection micro stereolithography (PµSL) [9-12] employing patterned UV

illumination, possess significantly improved printing resolution (<10 μm) [10] by carefully adjusting the laser beam diameters or magnification factors of projection optics. Instead of the voxelby-voxel laser scanning process of SLA, the PµSL parallelizes the 3D printing process in a layer-by-layer fashion, resulting in significant time savings with high-resolution 3D printing [10]. However, for both the SLA and PµSL processes, photocurable liquid resins are recoated onto previously solidified layers, and then photopolymerized by UV laser beam and patterned UV illumination. As a result, the waiting time for recoating is typically longer for high-viscosity resins, such as composite resins containing solid particles, which significantly constrain the printing speed ($\sim 0.57 \, \mu \text{m} \cdot \text{s}^{-1}$) [12]. For example, it takes 4.86 hours to fabricate a 1-cm-long structure [12]. Moreover, the delamination and movement of the printing platform will also cause printing inconsistencies and affect the homogeneity of the printed parts.

In the case of printing copper particle-reinforced PMCs, higher filler loading is preferred to guarantee satisfactory physical properties, such as mechanical strength, electrical and thermal conductivities, etc. However, this increases resins' viscosity tremendously, which makes the printing extremely time-consuming. On the other hand, because the interfacial interaction between the copper particles and the polymer matrix is relatively poor [13–15], the copper particles tend to agglomerate and precipitate, which leads to the separation between the copper particles and the polymer matrix in the resin when the filler loading is higher. This separation causes the loss of metal particles and inhomogeneity of the printed 3D structures.

Herein, to overcome these limitations, as illustrated in Figure 1, we present a new printing strategy for 3D copper structures by doping nanoporous copper (NP-Cu, prepared by a chemical dealloying process) powders (Figure 1a & 1b) with significantly increased surface area [16] into photopolymerizable polymer matrix. The new high-resolution and high-speeding printing method is termed micro-continuous liquid interface printing (µCLIP) [17]. By removing the delamination steps, µCLIP can dramatically decrease the fabrication time when dealing with high-viscosity resins, and consequently, overcome the particle-matrix separation challenge. To formulate stabilized PMC resins comprising higher loading of NP-Cu, a dispersant is introduced, and the composition is optimized for the µCLIP process. Then, 3D structures (termed green bodies) are printed from those optimized resins by µCLIP with optimal processing parameters [17]. After printing, the green bodies are composed of the unwelded NP-Cu powders and the polymer matrix. Besides, the NP-Cu powders are partially oxidized in the air. To degrade the polymer, deoxidize, and weld the powders, we sinter the green bodies in Ar/H₂ atmosphere. The temperature for the polymer degradation and the practical amount of NP-Cu powders' loss during the printing are characterized by thermogravimetric analysis (TGA) on the green bodies. The structures after sintering are termed sintered parts. To analyze the sintering results quantitively, the microstructures of green bodies and

sintered parts are characterized by scanning electrical microscope (SEM) and energy-dispersive X-ray spectroscopy (EDS). Moreover, the comparison of the resistivity between the green bodies and sintered parts is utilized to characterize the welding of the NP-Cu powders.

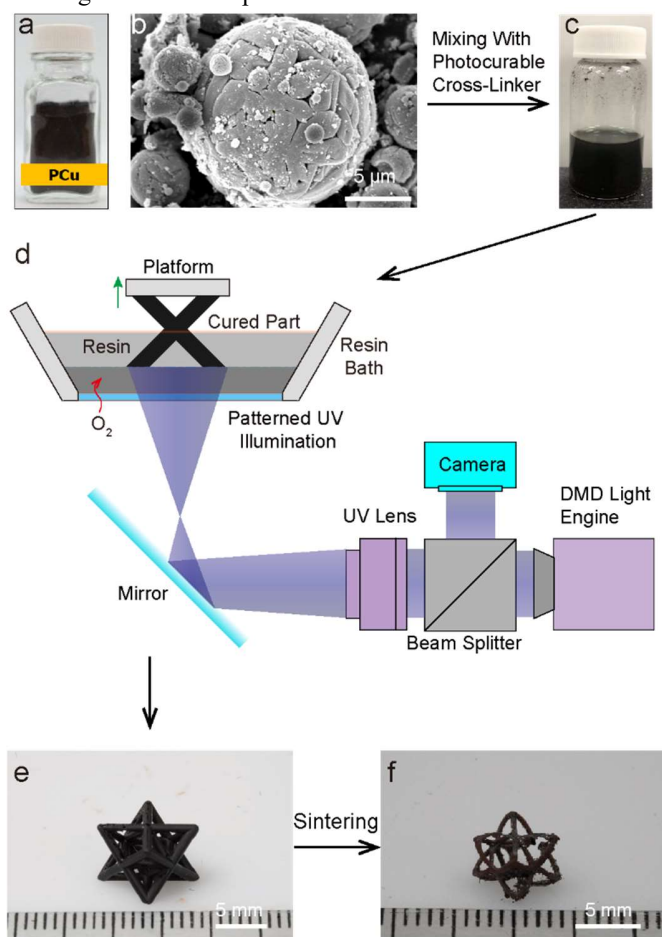


Figure 1: 3D PRINTING OF THE NANOPOROUS COPPER. (a) Optical image of the nanoporous copper powders. (b) SEM image of the nanoporous copper powders. (c) Optical image of the photocurable resin containing the 40 wt% NP-Cu powders. (d) Schematic illustration of the μCLIP system. (e) Optical image of the as-printed 3D structure. (f) Optical image of the sintered structures.

2. MATERIALS AND METHODS

2.1 Preparation of the nanoporous copper powders

Spherical Copper-Aluminum ($Cu_{33}Al_{67}$ in atomic fractions) gas atomized powders were purchased from Valimet Inc. Sodium hydroxide (NaOH, Reagent grade) was purchased from Sigma Aldrich. Anhydrous ethanol (Reagent grade) was purchased from Carolina. A 5000 ml glass beaker containing 2500 ml of freshly prepared 3M NaOH solution was placed on a hotplate. Due to the exothermic reaction of NaOH dissolution with water, the prepared solution naturally heated to 52 ± 1 °C. Then, the beaker with the solution was cool down to 45 °C naturally. After that, the solution was rapidly heated to 50 °C on a hotplate.

After reaching the desired temperature, CuAl powders were titrated into the NaOH solution at a rate of 1 g every 30 s with a total titration time of 24 min 30 s. After the titration, NP-Cu powders were kept for 5 additional minutes in the NaOH solution to complete Al etching. After finishing the etching, NP-Cu powders were first washed with 1 L DI water. Then, the powders were washed with 200 ml anhydrous ethanol. After the washing, powders were transferred to the vacuum oven in beakers and were dried at 90 °C for 24 h.

2.2 Photopolymerizable resin preparation

The photocurable resin for µCLIP consists of 54 wt% poly (ethylene glycol) diacrylate (PEGDA, Mn 700, Sigma Aldrich) as the photopolymerizable cross-linker, 4 wt% bis(2,4,6-trimethylbenzoyl)-phenylphosphineoxide (Sigma Aldrich, named as Irgacure 819 by BASF) as photoinitiator, 40 wt% NP-Cu powders as the metal material, and 2 wt% TEGO DISPERS 685 (EVONIK) as the dispersant to avoid the separation between the NP-Cu powders and the cross-linker. For preparation, Irgacure 819 and TEGO DISPERS 685 were first dissolved into PEGDA. Then, the solution was mixed with NP-Cu powders in a ball-milling machine (MA0101, MSE Supplies) for 24h.

To characterize the effect of the dispersant, the resin consisting of 56 wt% PEGDA, 4 wt% Irgacure 819, and 40 wt% NP-Cu powders was prepared by the identical method.

The resin without any NP-Cu was utilized as comparison, it contains 97.9 wt% PEGDA, 2 wt% Irgacure 819, and 0.1 wt% of 1-phenylazo-2-naphthol (Sudan 1, Sigma Aldrich) as the UV absorber was prepared by dissolving Irgacure 819 and Sudan 1 into PEGDA.

2.3 Micro continuous liquid interface printing (µCLIP)

The µCLIP system was employed to fabricate the NP-Cu green bodies. The CAD model of the green body was first sliced into a series of 2D grayscale bitmaps with a specific layer slicing thickness via a customized MATLAB program. The sliced bitmap patterns were then loaded into the light engine (PRO6600, Wintech Digital), and the dynamic mask generator for the projection of the bitmap was a digital micromirror device (Texas Instruments) with a resolution of 3840 × 2160. The projection optics of the printer was optimized to have a pixel resolution of 5.8 $\mu m \times 5.8 \mu m$ at the focal plane, which corresponds to a maximum build area for the system of 22.27 mm × 12.53 mm. The patterned UV illumination was projected onto the transparent window of the resin bath, and the liquid resin under the illuminated light (white pattern in the mask) would be polymerized into a solid layer. Simultaneously, the building platform mounted on a motorized translation stage (X-LSM200A-PTB2, Zaber Technology Inc.) was raised continuously. After printing, the green bodies were removed from the platform and cleaned with isopropanol (Sigma Aldrich).

2.4 Sintering process

After the printing, the green bodies were sintered in a 95% Ar/5% H_2 mixture atmosphere in a tube furnace (Carbolite-Gero CTF 12/75/700, Thermo Fisher Scientific) at varying temperatures. The sintering process is shown in **Figure 2**. First, the temperature was increased from room temperature to 460 °C gradually with a heating rate of 1.5 °C·min⁻¹ and then dwelled

for 10 hours for polymer degradation. Then the temperature was raised up to 500 °C gradually with a heating rate of 1.5 °C·min¹ and then dwelled for 5 hours for NP-Cu powders' welding and deoxidation. Finally, the furnace was cooled to room temperature with a cooling rate of 1.5 °C·min¹¹.

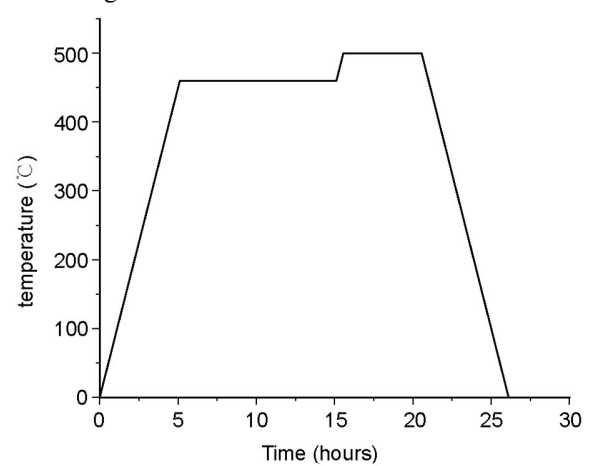


Figure 2: TEMPERATURE CHART OF THE SINTERING PROCESS.

2.5 Characterization

Thermogravimetric (TGA) diagrams of the green bodies were measured by TGA 550 (TA instrument). In detail, each asprinted green body with weight of 10-20 mg was heated to 550 °C at a rate of 5 °C·min⁻¹ in the nitrogen atmosphere.

The microstructures of the green bodies and sintered parts were characterized by using scanning electron microscopes (SEM) (Helios 5 UX, Thermo Fisher Scientific) with an accelerating voltage of 5 kV. The element contents of the green bodies and sintered parts were measured by using the energy-dispersive X-ray spectroscopy (EDS) function of this scanning electron microscope with an accelerating voltage of 20 kV.

Mirrorless Digital Camera 24.3 MP SLR Camera (Alpha6100, Sony) with a macro lens (FE 2.8/90 MACRO G OSS, Sony) was utilized to acquire optical images of the asprinted green bodies and sintered parts.

3. RESULTS AND DISCUSSION

Our new printing strategy's first step is preparing stable photocurable resins. In detail, Poly (ethylene glycol) diacrylate (PEGDA, Mn 700) was chosen as the photopolymerizable cross-Bis(2,4,6-trimethylbenzoyl)-phenylphosphineoxide linker. (Irgacure 819) was chosen as the UV photoinitiator. Nanoporous copper (NP-Cu) powders (Figure 1a & 1b) which were fabricated by a chemical dealloying process [18] (Materials and Methods) were chosen as the metal material. To avoid the separation between the NP-Cu powders and the cross-linker, TEGO DISPERS 685 was used as the dispersant. By the introduction of the dispersant, the resin can be stabilized with filler loading up to 40 wt%, as shown in Figure 1c. After that, to rapidly fabricate green bodies featuring sophisticated geometries, custom-made high-resolution micro-continuous liquid interface printing (µCLIP) was introduced as a versatile manufacturing technology that overcame the limitations such as

the relatively low printing resolution associated with extrusionbased approaches and the relatively low printing speed associated with traditional vat photopolymerization-based methods [10]. In the µCLIP system, a transparent oxygenpermeable membrane is mounted below the resin bath as shown in Figure 1d, which creates a thin polymerization-free "dead zone" between the membrane and the cured part because of the inhibition of photopolymerization induced by oxygen in the atmosphere [17,19-21]. This unpolymerized liquid interface facilitates continuous printing and dramatically increases the fabrication speed up to 250 μm·s⁻¹ [20]. For printing, the CAD model of the green body is first sliced into a series of 2D grayscale bitmaps with a layer slicing thickness of 5 µm along the printing direction. Then, the sliced bitmap patterns are loaded into a light engine with an illuminating wavelength of 385 nm. The patterned UV light is projected onto the oxygen-permeable membrane with desired light intensity and pixel size. Under the illumination of the patterned UV light, the photopolymerizable resin above the "dead zone" is selectively polymerized into solid and the platform is continuously moved upward from the focal plane at the desired speed synchronously [21]. Figure 1e shows a green body with the octet truss structure printed with the speed of 10 μ m·s⁻¹ under the illumination with a light intensity of ~10 mW·cm⁻². The green body is composed of NP-Cu particlereinforced polymer matrix. Besides, the NP-Cu powders in the polymer matrix are partially oxidized because the atmosphere for the chemical dealloying and printing is air [22]. To obtain 3D copper structures with minimized oxidation, we sintered the green bodies in the Ar/H₂ atmosphere. The specific sintering program is shown in Figure 2. Figure 1f shows the optical image of the sintered part. It can be noted that after sintering, there is an expected shrinkage and the color is changed, due to the polymer degradation and NP-Cu powders' deoxidation.

3.1 Characterization of as-printed green bodies

To characterize the remaining NP-Cu powders in the asprinted green bodies, we print samples with identical octet truss structure from different resins. Figure 3a-3c show green bodies printed from three different resins, including (I) the resin with 0 wt% NP-Cu, (II) the resin comprising 40 wt% NP-Cu without dispersant, and (III) the resin comprising 40 wt% NP-Cu with 2 wt% dispersant, respectively (Materials and Methods). After printing, thermogravimetric analysis (TGA) was utilized to quantitively characterize the remaining NP-Cu powders in different as-printed green bodies, which is shown in Figure 3d-3f. For the green body printed from the resin without NP-Cu powders (Figure 3a), the remaining weight percentage is close to 0 wt%, as shown in Figure 3d. For the green body printed from the resin comprising 40 wt% NP-Cu powders without dispersant, the color is inhomogeneous, and the printing fails, as shown in Figure 3b. Correspondingly, the TGA result of this green body in Figure 3e shows that the remaining weight percentage is only 17 wt%. This is because the separation between the NP-Cu powders and the PEGDA in the photocurable resin during printing. Due to the separation, NP-Cu powders agglomerate and precipitate at the bottom of the resin bath, after which only the PEGDA containing a small quantity of NP-Cu

powders is cured on the printing platform. Thus, the remaining weight percentage of NP-Cu powders in the as-printed green bodies significantly decreases compared to the as-prepared photocurable resin. Moreover, with the gradual precipitation of the partially oxidized black NP-Cu powders during printing, the patterned UV light is absorbed and cannot further activate the photopolymerization. As a result, the printed structure is fragmentary, as shown in Figure 3b. On the contrary, the green body printed from the resin comprising 40 wt% of NP-Cu powders with 2% dispersant shows a homogeneous color visually, and the remaining weight percentage is 39 wt%, indicating that there is scarcely any loss of NP-Cu due to introducing the dispersant, as shown in Figure 3c & 3f. All these results verify that the dispersant can avoid the separation of resin during printing, which increases the amount of remaining NP-Cu in the green bodies. Besides, for all aforementioned green bodies, the polymer degradation ends at ~420 °C. Thus, we choose 460°C as the degradation temperature in the sintering process.

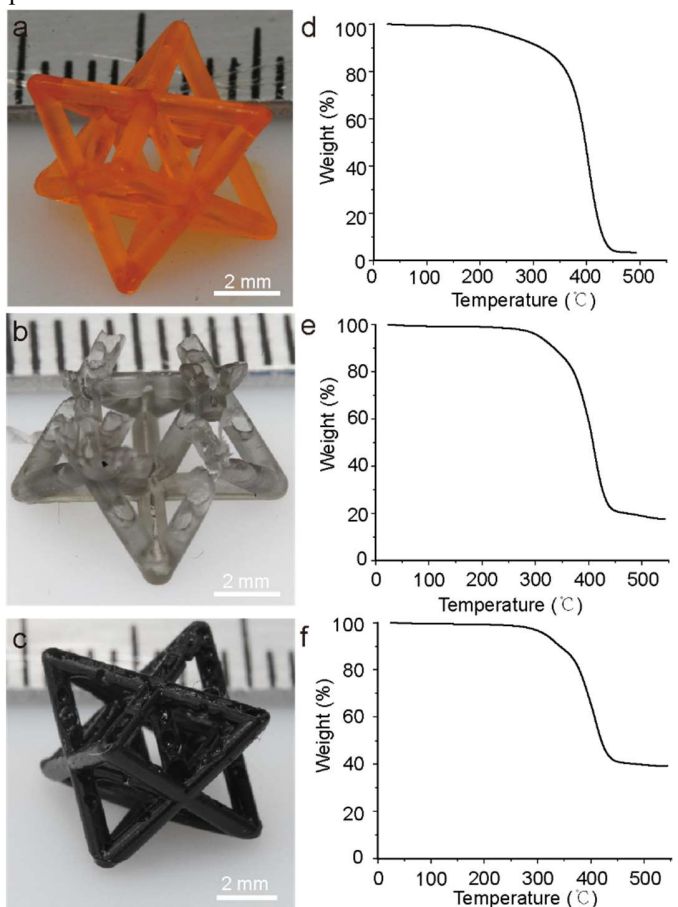


Figure 3: CHARACTERIZATION OF AS-PRINTED 3D STRUCTURES. Optical images of the green bodies printed from the resin composed of 0 wt% NP-Cu powders (a), the resin comprising 40 wt% NP-Cu powders with 0 wt% dispersant (b), and the resin comprising 40 wt% NP-Cu powders with 2 wt% dispersant (c). And the corresponding TGA diagram of the asprinted green bodies (d-f).

3.2 Characterization of the as-printed and sintered parts

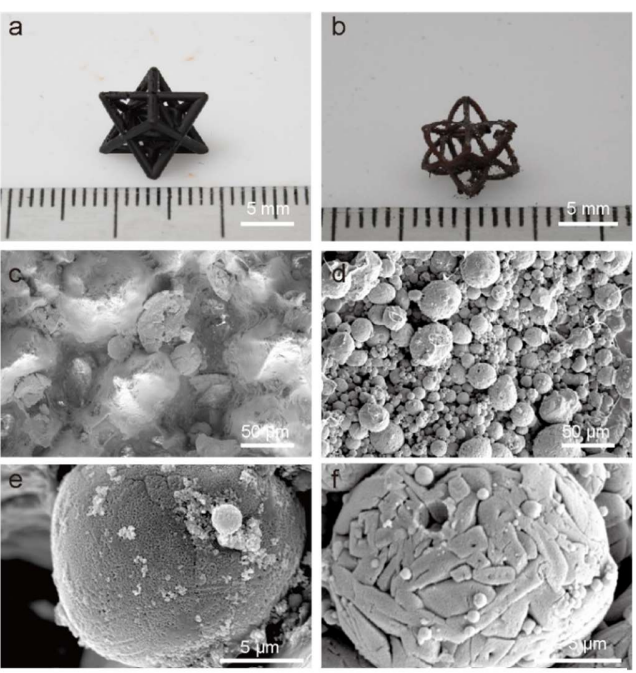


Figure 4: MORPHOLOGY CHARACTERIZATIONS OF AS-PRINTED AND SINTERED PARTS. Optical image of the green body (a) and the sintered part (b). SEM images of the as-printed green body (c & e), and sintered parts (d & f).

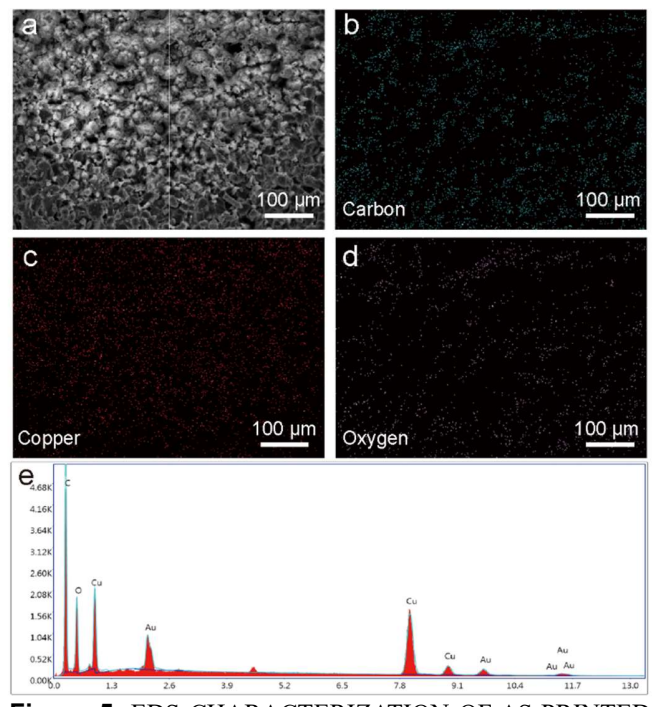


Figure 5: EDS CHARACTERIZATION OF AS-PRINTED PARTS. (a) SEM image of the as-printed green body. EDS mapping of carbon (b), copper (c), and oxygen (d) in the green body. (e) EDS spectrum of the green body.

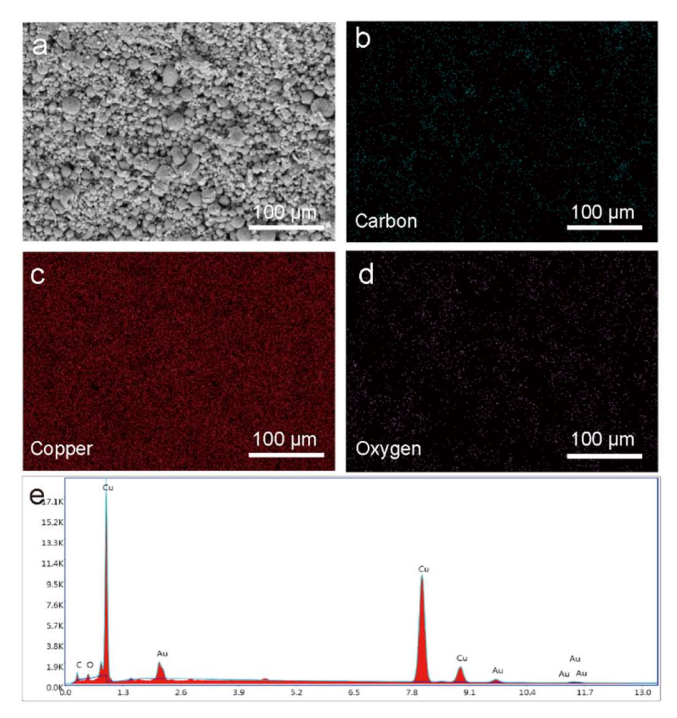


Figure 6: EDS CHARACTERIZATION OF SINTERED PARTS. (a) SEM image of the sintered part. EDS mapping of carbon (b), copper (c), and oxygen (d) in the sintered part. (e) EDS spectrum of the sintered part.

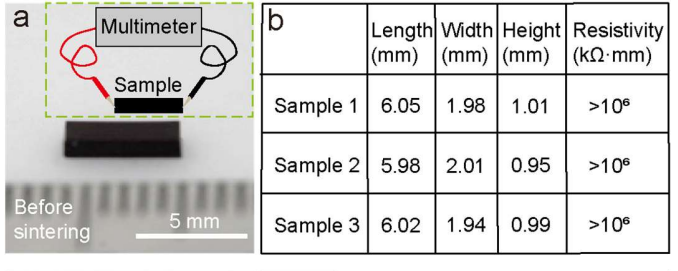
To obtain 3D copper structures with minimized oxidation caused by the air atmosphere of the chemical dealloying and printing process [22], in the sintering, after the polymer degradation process for 10 hours at 460°C, the samples were continued to heat to 500 °C in the Ar/H₂ atmosphere. Theoretically, at 500 °C, the NP-Cu powders are deoxidized and welded with each other [23]. Figure 4a & 4b show an as-printed green body and a sintered part, respectively. Visually, there is an expected shrinkage, and the color is changed after sintering. For quantitative verification, scanning electrical microscope (SEM) images and energy-dispersive X-ray spectroscopy analysis for green bodies and sintered parts were then utilized (Figure 4-7). In the green body, the nanoporous copper powders are inlaid in the polymer matrix, as shown in Figure 4c & 4e. Correspondingly, the atomic ratio of carbon (the component of the polymer matrix) and oxygen (the component of the polymer matrix and partially oxidized NP-Cu powders) is 72.70 % and 16.14 %, respectively, as shown in the EDS analysis in Figure 5a-5e & 7. After sintering, the NP-Cu powders are bridged across particle-to-particle interfaces and the polymer matrix disappears, as shown in Figure 4d & 4f. EDS results, as shown in Figure 6a-6e & 7, show that after sintering the atomic ratio of carbon and oxygen decreases to 16.83 % and 2.31%, respectively. All these results indicate that the polymer is degraded, and the NP-Cu powders are deoxidized partially during the sintering. However, carbon and oxygen elements still exist after sintering, as shown in Figure 6a-6e & 7, indicating that there are remaining polymers and oxidized particles after

sintering. Moreover, for the welding of the NP-Cu powders, because SEM images can only achieve visual characterization, a quantitative characterization method is still necessary.

Elements	Atomic %	
	Green body	Sintered part
С	72.70	16.83
0	16.14	2.31
Cu	9.59	77.18
Au	1.58	3.68

Figure 7: ATOMIC RATIO OF THE ELEMENTS IN THE GREEN BODY AND SINTERED PART.

3.3 Resistivity measurement



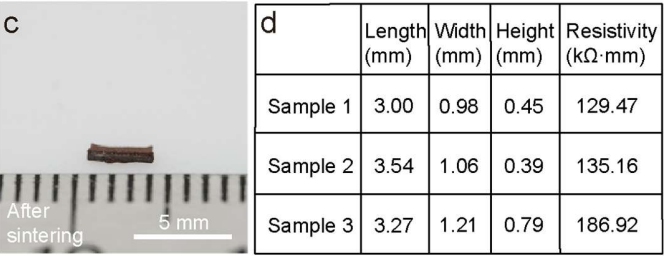


Figure 8: MEASUREMENT OF RESISTIVITY. Optical images of the as-printed green body (a) and sintered part (c) for measuring the resistivity. Geometry parameters and measured resistivity of as-printed green bodies (b) and sintered parts (d).

The resistivity of the green bodies and the sintered parts were measured and compared. A two-point probe method was utilized to measure the resistance of samples with cuboid structures, as shown in **Figure 8a & 8c**. Then, the resistivity (ρ) of the samples was calculated by

$$\rho = R \frac{W \dot{H}}{L} \tag{1}$$

in which R is the measured resistance, W, H and L is the measured width, height, and length of the sample, respectively. As shown in **Figure 8b & 8d**, after the sintering, the average resistivity of the samples significantly decreases from $1~\rm G\Omega \cdot mm$ to $150~\rm k\Omega \cdot mm$ because the NP-Cu powders weld with each other and the concentration of polymer and oxidized NP-Cu powders decreases. However, the resistivity is still larger than the solid pure copper because the polymer matrix is degraded and the NP-Cu powders are deoxidized partially, as shown in **Figure 6a-6e**

& 7. To thoroughly degrade the polymers and deoxidize the powders, our future work will focus on the optimization of the powder preparation processes and the sintering process.

4. CONCLUSION

In conclusion, we have demonstrated a new strategy for rapid 3D printing of NP-Cu structures via $\mu CLIP$. The stability of the printing resin has been optimized by introducing the dispersant to avoid the separation of the solid fillers during the printing. The printed structures were then sintered. After sintering, 3D copper structures comprising 77.18 atomic% of Cu element were obtained. Besides, the structures manifest an average resistivity of 150 k Ω ·mm at room temperature. Our future work will focus on further deoxidation of the NP-Cu powders and degradation of the polymers. We envision that this new strategy not only potentially benefits the rapid printing of 3D copper structures, but also provides insights that are useful in fabricating components with other metal materials in higher resolution and shorter fabrication time.

ACKNOWLEDGEMENTS

This work is funded by the National Science Foundation (NSF) Grant No. CMMI 1932899. The authors thank Prof. Kenan Song for help with the TGA measurement. The authors also acknowledge the Eyring Materials Center at Arizona State University.

REFERENCES

- [1] Buchanan, C., and Gardner, L., 2019, "Metal 3D Printing in Construction: A Review of Methods, Research, Applications, Opportunities and Challenges," Engineering Structures, 180, pp. 332–348.
- [2] Hasib, A. G., Niauzorau, S., Xu, W., Niverty, S., Kublik, N., Williams, J., Chawla, N., Song, K., and Azeredo, B., 2021, "Rheology Scaling of Spherical Metal Powders Dispersed in Thermoplastics and Its Correlation to the Extrudability of Filaments for 3D Printing," Additive Manufacturing, 41, p. 101967.
- [3] Boparai, K. S., Singh, R., and Singh, H., 2016, "Development of Rapid Tooling Using Fused Deposition Modeling: A Review," RPJ, **22**(2), pp. 281–299.
- [4] Roy, N. K., Behera, D., Dibua, O. G., Foong, C. S., and Cullinan, M. A., 2019, "A Novel Microscale Selective Laser Sintering (μ-SLS) Process for the Fabrication of Microelectronic Parts," Microsyst Nanoeng, 5(1), p. 64.
- [5] Heigel, J. C., Michaleris, P., and Reutzel, E. W., 2015, "Thermo-Mechanical Model Development and Validation of Directed Energy Deposition Additive Manufacturing of Ti-6Al-4V," Additive Manufacturing, 5, pp. 9–19.
- [6] Fayazfar, H., Salarian, M., Rogalsky, A., Sarker, D., Russo, P., Paserin, V., and Toyserkani, E., 2018, "A Critical Review of Powder-Based Additive

- Manufacturing of Ferrous Alloys: Process Parameters, Microstructure and Mechanical Properties," Materials & Design, **144**, pp. 98–128.
- [7] Bhattacharjee, N., Parra-Cabrera, C., Kim, Y. T., Kuo, A. P., and Folch, A., 2018, "Desktop-Stereolithography 3D-Printing of a Poly(Dimethylsiloxane)-Based Material with Sylgard-184 Properties," Adv. Mater., **30**(22), p. 1800001.
- [8] Phillips, B. T., Allder, J., Bolan, G., Nagle, R. S., Redington, A., Hellebrekers, T., Borden, J., Pawlenko, N., and Licht, S., 2020, "Additive Manufacturing Aboard a Moving Vessel at Sea Using Passively Stabilized Stereolithography (SLA) 3D Printing," Additive Manufacturing, 31, p. 100969.
- [9] Chen, X., Ware, H. O. T., Baker, E., Chu, W., Hu, J., and Sun, C., 2017, "The Development of an All-Polymer-Based Piezoelectric Photocurable Resin for Additive Manufacturing," Procedia CIRP, 65, pp. 157–162.
- [10] Chen, X., Liu, W., Dong, B., Lee, J., Ware, H. O. T., Zhang, H. F., and Sun, C., 2018, "High-Speed 3D Printing of Millimeter-Size Customized Aspheric Imaging Lenses with Sub 7 Nm Surface Roughness," Adv. Mater., 30(18), p. 1705683.
- [11] Li, X., Yang, Y., Liu, L., Chen, Y., Chu, M., Sun, H., Shan, W., and Chen, Y., 2020, "3D-Printed Cactus-Inspired Spine Structures for Highly Efficient Water Collection," Adv. Mater. Interfaces, 7(3), p. 1901752.
- [12] Li, X., Yuan, Y., Liu, L., Leung, Y.-S., Chen, Y., Guo, Y., Chai, Y., and Chen, Y., 2020, "3D Printing of Hydroxyapatite/Tricalcium Phosphate Scaffold with Hierarchical Porous Structure for Bone Regeneration," Bio-des. Manuf., 3(1), pp. 15–29.
- [13] Rong, M. Z., Zhang, M. Q., and Ruan, W. H., 2006, "Surface Modification of Nanoscale Fillers for Improving Properties of Polymer Nanocomposites: A Review," Materials Science and Technology, 22(7), pp. 787–796.
- [14] Liu, S., Wang, W., Xu, W., Liu, L., Zhang, W., Song, K., and Chen, X., 2022, "Continuous Three-Dimensional Printing of Architected Piezoelectric Sensors in Minutes," Research, 2022, pp. 1–13.
- [15] Hamming, L. M., Qiao, R., Messersmith, P. B., and Catherine Brinson, L., 2009, "Effects of Dispersion and Interfacial Modification on the Macroscale Properties of TiO2 Polymer–Matrix Nanocomposites," Composites Science and Technology, **69**(11–12), pp. 1880–1886.
- [16] Detsi, E., De Jong, E., Zinchenko, A., Vuković, Z., Vuković, I., Punzhin, S., Loos, K., ten Brinke, G., De Raedt, H. A., Onck, P. R., and De Hosson, J. T. M.,

- 2011, "On the Specific Surface Area of Nanoporous Materials," Acta Materialia, **59**(20), pp. 7488–7497.
- [17] Tumbleston, J. R., Shirvanyants, D., Ermoshkin, N., Janusziewicz, R., Johnson, A. R., Kelly, D., Chen, K., Pinschmidt, R., Rolland, J. P., Ermoshkin, A., Samulski, E. T., and DeSimone, J. M., 2015, "Continuous Liquid Interface Production of 3D Objects," Science, 347(6228), pp. 1349–1352.
- [18] Zhang, Y., Sun, X., Nomura, N., and Fujita, T., 2019, "Hierarchical Nanoporous Copper Architectures via 3D Printing Technique for Highly Efficient Catalysts," Small, **15**(22), p. 1805432.
- [19] Liu, L., Liu, S., Schelp, M., and Chen, X., 2021, "Rapid 3D Printing of Bioinspired Hybrid Structures for High-Efficiency Fog Collection and Water Transportation," ACS Appl. Mater. Interfaces, **13**(24), pp. 29122–29129.
- [20] Shao, G., Hai, R., and Sun, C., 2020, "3D Printing Customized Optical Lens in Minutes," Adv. Optical Mater., **8**(4), p. 1901646.
- [21] Ware, H. O. T., and Sun, C., 2019, "Method for Attaining Dimensionally Accurate Conditions for High-Resolution Three-Dimensional Printing Ceramic Composite Structures Using MicroCLIP Process," Journal of Micro and Nano-Manufacturing, 7(3), p. 031001.
- [22] Wang, Z., Wang, L., Qin, C., Liu, J., Li, Y., and Zhao, W., 2014, "Tailored Dealloying Products of Cu-Based Metallic Glasses in Hydrochloric Acid Solutions," Mat. Res., 17(4), pp. 1003–1009.
- [23] Kim, J. Y., Rodriguez, J. A., Hanson, J. C., Frenkel, A. I., and Lee, P. L., 2003, "Reduction of CuO and Cu₂ O with H₂: H Embedding and Kinetic Effects in the Formation of Suboxides," J. Am. Chem. Soc., **125**(35), pp. 10684–10692.